pp solar neutrinos at DARWIN

André de Gouvêa,[1] Emma McGinness,[2,3] Ivan Martinez-Soler,[1,4,5,6] and Yuber F. Perez-Gonzalez[1,4,5,7]

[1]*Northwestern University, Department of Physics & Astronomy, 2145 Sheridan Road, Evanston, Illinois 60208, USA*
[2]*University of California Berkeley, Department of Physics, 366 Physics North, Berkeley, California 94720, USA*
[3]*University of California Berkeley, Department of Astronomy, 501 Campbell Hall, Berkeley, California 94720, USA*
[4]*Colegio de Fsica Fundamental e Interdisciplinaria de las Amricas (COFI) 254 Norzagaray street, San Juan, Puerto Rico 00901, USA*
[5]*Theoretical Physics Department, Fermilab, P.O. Box 500, Batavia, Illinois 60510, USA*
[6]*Department of Physics & Laboratory for Particle Physics and Cosmology, Harvard University, Cambridge, Massachusetts 02138, USA*
[7]*Institute for Particle Physics Phenomenology, Durham University, South Road, Durham DH1 3LE, United Kingdom*

(Received 21 November 2021; accepted 26 October 2022; published 17 November 2022)

The DARWIN collaboration recently argued that DARWIN (dark matter wimp search with liquid xenon) can collect, via neutrino-electron scattering, a large, useful sample of solar pp-neutrinos, and measure their survival probability with subpercent precision. We explore the physics potential of such a sample in more detail. We estimate that, with 300 ton-years of data, DARWIN can also measure, with the help of current solar neutrino data, the value of $\sin^2\theta_{13}$, with the potential to exclude $\sin^2\theta_{13} = 0$ close to the three-sigma level. We explore in some detail how well DARWIN can constrain the existence of a new neutrino mass-eigenstate ν_4 that is quasimass-degenerate with ν_1 and find that DARWIN's sensitivity supersedes that of all current and near-future searches for new, very light neutrinos. In particular, DARWIN can test the hypothesis that ν_1 is a pseudo-Dirac fermion as long as the induced mass-squared difference is larger than 10^{-13} eV^2, one order of magnitude more sensitive than existing constraints. Throughout, we allowed for the hypotheses that DARWIN is filled with natural xenon or ^{136}Xe-depleted xenon.

DOI: 10.1103/PhysRevD.106.096017

I. INTRODUCTION

Multiton-scale, next-generation dark matter experiments are expected to collect significant statistics of atmospheric and solar neutrinos. The DARWIN collaboration recently argued that DARWIN (dark matter wimp search with liquid xenon) can collect a large, useful sample of solar pp-neutrinos, measured via elastic neutrino–electron scattering [1]. There, they argued that the survival probability of pp-neutrinos can be measured with subpercent precision and that one can measure the Weinberg angle at low momentum transfers with 10% precision, independent from the values of the neutrino oscillation parameters. Here, we explore other neutrino-physics-related information one can obtain from a high-statistics, high-precision measurement of the pp-neutrino flux.

In a nutshell, pp-neutrinos are produced in the solar core via proton-proton fusion: $p + p \to {}^2\mathrm{H} + e^+ + \nu$. The vast majority of neutrinos produced by the fusion cycle that powers our Sun are produced via proton-proton fusion. pp-neutrinos have the lowest energy among all solar neutrino "types" (other types include pep-neutrinos, ^{7}Be-neutrinos, ^{8}B-neutrinos, and CNO-neutrinos) and are characterized by a continuous spectrum that peaks around 300 keV and terminates around 420 keV. Theoretically, the pp-neutrino flux is known at better than the percent level [2] given they are created early in the pp-fusion cycle—they are the first link in the chain—and their flux is highly correlated with the photon flux, measured with exquisite precision. For the sake of comparison, the flux of ^{7}Be-neutrinos and ^{8}B-neutrinos, which provide virtually all information on the particle-physics properties of solar neutrinos, can be computed at, approximately, the 6% and 12% level, respectively [3,4]. The pp-neutrino flux has been directly measured, independent from the other flux-types, by the Borexino collaboration [5], with 10% precision.

A percent-level measurement of the pp-neutrino flux is expected to be sensitive to new-physics effects in neutrino

physics that are also at the percent level. This includes, for example, effects from the so-called reactor angle θ_{13}—not new physics but very small for solar neutrinos—and the presence of new neutrino states or neutrino interactions. Furthermore, the fact that pp-neutrinos have energies that are significantly lower than those of the other solar neutrino types renders them especially well-suited to constrain (or discover) new, very long oscillation lengths associate to very small new neutrino mass-squared differences. These searches are expected to add significantly to our ability to test the hypothesis that the neutrinos are pseudo-Dirac fermions [6–8] (for relevant recent discussions, see, for example, [9–12]). Here, as far as new-physics hypotheses are concerned, we concentrate on the search for new, very light neutrino states.

In Sec. II, we review the relevant features of the proposed DARWIN experiment and provide information on how we simulate and analyze DARWIN data on pp-neutrinos. In Sec. III, we show that a percent-level measurement of the pp-neutrino flux allows for a "solar-neutrinos-only" measurement of $\sin^2\theta_{13}$. In Sec. IV, we compute the sensitivity of DARWIN to the hypothesis that there is a fourth neutrino with a mass m_4 that is quasidegenerate with the mass of the first neutrino state, m_1 (in the Appendix, we discuss how this can be generalized). We concentrate on the region of parameter space where the new mass-squared difference is $10^{-13}\ \text{eV}^2 \lesssim |m_4^2 - m_1^2| \lesssim 10^{-6}\ \text{eV}^2$. We add some concluding remarks in Sec. V.

II. DARWIN AS A LOW-ENERGY SOLAR NEUTRINO EXPERIMENT

DARWIN is projected to be a large—30 tons fiducial volume—liquid xenon time-projection chamber, aimed at searching for weakly interacting massive particles (WIMP) in the GeV to TeV mass range [13] via elastic WIMP–nucleon scattering. It will inevitably be exposed to a large flux of solar and atmospheric neutrinos and is large enough that solar-neutrino scattering events will occur at an observable rate.

According to [1], DARWIN is expected to collect a sample of almost ten thousand pp-neutrinos per year via elastic neutrino–electron scattering:

$$\nu_\alpha + e^- \to \nu_\alpha + e^-, \tag{2.1}$$

where $\alpha = e, \mu, \tau$ is the flavor of the incoming neutrino. The flavor of the outgoing neutrinos is, of course, never observed. For pp-neutrino energies, the cross section for $\nu_e e$-scattering is around six times larger than that of $\nu_a e$-scattering, $a = \tau, \mu$ and the differences between the cross sections for $\nu_\mu e$-scattering and $\nu_\tau e$-scattering are negligible. At leading order in the weak interactions, the differential cross section in the rest frame of the electron is

$$\frac{\mathrm{d}\sigma}{\mathrm{d}T}(\nu_\alpha + e^- \to \nu_\alpha + e^-) = \frac{2G_F^2 m_e}{\pi}\left[a_\alpha^2 + b_\alpha^2\left(1 - \frac{T}{E_\nu}\right)^2 - a_\alpha b_\alpha \frac{T}{E_\nu}\right], \tag{2.2}$$

where T is the kinetic energy of the recoil electron, E_ν is the incoming neutrino energy, m_e is the electron mass and G_F is the Fermi constant. The dimensionless couplings a_α, b_α are

$$a_e = -\frac{1}{2} - \sin^2\theta_W, \qquad b_e = -\sin^2\theta_W;$$
$$a_a = \frac{1}{2} - \sin^2\theta_W, \qquad b_a = -\sin^2\theta_W, \tag{2.3}$$

where θ_W is the weak mixing angle. DARWIN measures the kinetic energy spectrum of the recoil electrons.

If filled with natural xenon, one expects a large number of electron-events in the energy range of interest from the double-beta decays of ^{136}Xe. These events are a powerful source of background for solar-neutrino studies and, according to [1], obviate the study of solar neutrinos with energies higher than 1 MeV. They are a powerful nuisance for measurements of the ^{7}Be-neutrino flux and have a significant but not decisive impact on the measurement of the pp-neutrinos (around a 30% decrease in the precision with which the overall pp-neutrino flux can be measured [1]). The reason one can measure the pp-neutrino flux in spite of the ^{136}Xe background is that the shape of this particular background is well known and the experiment can detect events over a large range of recoil-electron energies, effectively measuring it with excellent precision. There is the possibility of filling DARWIN with liquid xenon depleted of the double-beta-decaying ^{136}Xe isotope. This would allow the study of higher energy solar neutrinos. Here we consider these two different scenarios, i.e., the ^{136}Xe-depleted version of DARWIN and the one where the abundance of ^{136}Xe agrees with natural expectations.

Other than the background from ^{136}Xe, for pp-neutrinos, the double electron capture decay of ^{124}Xe leads to three narrow peaks at 64.3 keV, 36.7 keV and 9.8 keV [1] and, at higher recoil energies, radioactive backgrounds from the detector components and the liquid volume supersede the pp-neutrino events for recoil kinetic energies above 200 keV or so. When simulating DARWIN data, we restrict our sample to events with recoil kinetic energies below 220 keV and assume that, in this energy range, the only sources of background are those from ^{136}Xe and ^{124}Xe. To simulate the background, we have used the information provided in [1]

When analyzing the simulated data, we marginalize over the normalization of the three ^{124}Xe lines, which we treat as free parameters, and the normalization of the ^{136}Xe recoil spectrum, which we assume is independently measured

with $\sigma_{136} = 0.1\%$ precision. The detection of ^{136}Xe by DARWIN extends to the MeV region, and its measurement at higher energies than the pp-neutrino flux will allow a sub-percent determination its normalization. We assume the shape of the ^{136}Xe recoil spectrum is known with infinite precision. For the ^{136}Xe-depleted version of DARWIN, we assume the ^{136}Xe-background is 1% of the background presented in [1]. We organize the simulated data into recoil-kinetic-energy bins with 10 keV width, consistent with the recoil-kinetic-energy resolution quoted in [1], starting at 1 keV. The large number of pp-neutrinos expected in DARWIN permits the use of a Gaussian χ^2 in order to address questions associated to the sensitivity of DARWIN to different oscillation hypothesis ($\mathcal{O}$),

$$\chi^2 = \frac{\left((1+f_{pp})E^{pp}(\mathcal{O}) + (N_{124}-1)^{124}\mathrm{Xe} + (\mathrm{N}_{136}-1)^{136}\mathrm{Xe} - \mathrm{E}^{\mathrm{pp}}(\mathcal{O}^{\mathrm{bch}})\right)^2}{E^{pp}(o^{bch}) + {}^{124}\mathrm{Xe} + {}^{136}\mathrm{Xe}} + \left(\frac{(N_{136}-1)}{\sigma_{136}}\right)^2 + \left(\frac{f_{pp}}{\sigma_{pp}}\right)^2, \quad (2.4)$$

where $E^{pp}(\mathcal{O})$ corresponds to the expected number of events under the neutrino-oscillation hypothesis "$\mathcal{O}$". In the benchmark scenario "$\mathcal{O}^{bch}$", the event distribution reproduces [1]. The knowledge over the normalization of ^{136}Xe is introduced into the χ^2-test by a Gaussian prior. f_{pp} and $\sigma_{pp} = 0.6\%$ indicate the pull parameter and normalization systematic uncertainty related the pp–neutrino flux, respectively. When applicable, we also use external priors on the known oscillation parameters, which have already been measured with known precision.

III. TESTING THE THREE-MASSIVE-NEUTRINOS PARADIGM

In the absence of more new physics, existing data reveals that the neutrino weak-interaction-eigenstates ν_α, $\alpha = e, \mu, \tau$, are linear combinations of the neutrino mass-eigenstates ν_i with mass m_i, $i = 1, 2, 3$:

$$\nu_\alpha = U_{\alpha i}\nu_i, \quad (3.1)$$

where the $U_{\alpha i}$, $\alpha = e, \mu, \tau$, $i = 1, 2, 3$, define the elements of a unitary matrix. Here, we are only interested in solar neutrinos so all accessible observables are sensitive to $|U_{ei}|^2$, $i = 1, 2, 3$. These, in turn, are parameterized with two mixing angles, θ_{12} and θ_{13}. Following the parametrization of the Particle Data Group [14],

$$|U_{e2}|^2 = \sin^2\theta_{12}\cos^2\theta_{13}, \qquad |U_{e3}|^2 = \sin^2\theta_{13}, \quad (3.2)$$

and unitarity uniquely determines the third matrix-element-squared: $|U_{e1}|^2 = 1 - |U_{e2}|^2 - |U_{e3}|^2$. Combined fits to the existing data reveal that the two independent mass-squared differences are $\Delta m^2_{21} \equiv m_2^2 - m_1^2 \sim 10^{-4}$ eV^2 and $|\Delta m^2_{31}| \equiv m_3^2 - m_1^2 \sim 10^{-3}$ eV^2. For more precise values see, for example, [15].[1] While Δm^2_{21} is defined to be positive, the sign of Δm^2_{31} is still unknown; for our purposes here, it turns out, this is irrelevant. The two mixing parameters of interest have been measured quite precisely. According to [15], at the one-sigma level,

$$\sin^2\theta_{12} = 0.304^{+0.013}_{-0.012}, \qquad \sin^2\theta_{13} = 0.02221^{+0.00068}_{-0.00062}. \quad (3.3)$$

The experiments that contribute most to these two measurements are qualitatively different. θ_{12} is best constrained by solar neutrino experiments—and is often referred to as the "solar angle"—while θ_{13} is best constrained by reactor antineutrino experiments—and is often referred to as the "reactor angle."

We are interested in the solar pp-neutrinos. These have a continuous energy spectrum that peaks around 300 keV and terminates at around 420 keV. The matter-potential $V = \sqrt{2}G_F N_e$, where G_F is the Fermi constant and N_e is the electron number-density, inside the Sun is $V_\odot < 2 \times 10^{-5}$ (eV^2/MeV) so, for neutrino energies $E < 0.420$ MeV, $|\Delta m^2_{21}|/(2E), |\Delta m^2_{31}|/(2E) \gg V_\odot$.[2] This, in turn, implies that, given what is known about the neutrino mass-squared differences, matter effects can be neglected. Including the fact that, for all practical purposes, solar neutrinos lose flavor coherence as they find their way from the Sun to the Earth, it is trivial to show that the ν_e survival probability is energy independent and given by

$$P_{ee} = |U_{e1}|^4 + |U_{e2}|^4 + |U_{e3}|^4. \quad (3.4)$$

On the other hand, solar neutrino experiments cannot distinguish ν_μ from ν_τ—the neutrino energies are too small—but are potentially sensitive to the combination $P_{ea} \equiv P_{e\mu} + P_{e\tau}$. In the three-massive-neutrinos paradigm

$$P_{ea} = 1 - P_{ee}. \quad (3.5)$$

Given our current knowledge of mixing parameters, for pp-neutrinos, we can indirectly infer that $P_{ee} = 0.552 \pm 0.025$, naively combining the uncertainties in Eq. (3.3) in quadrature.

According to [1], after 20 ton-years of exposure, DARWIN can measure P_{ee} with better than 1% accuracy.

[1] See also http://www.nu-fit.org.

[2] For example, at the center of the Sun, for neutrino energies less than 420 keV, the "matter equivalent" of $\sin^2 2\theta_{12}$ differs from its vacuum counterpart by less than one percent.

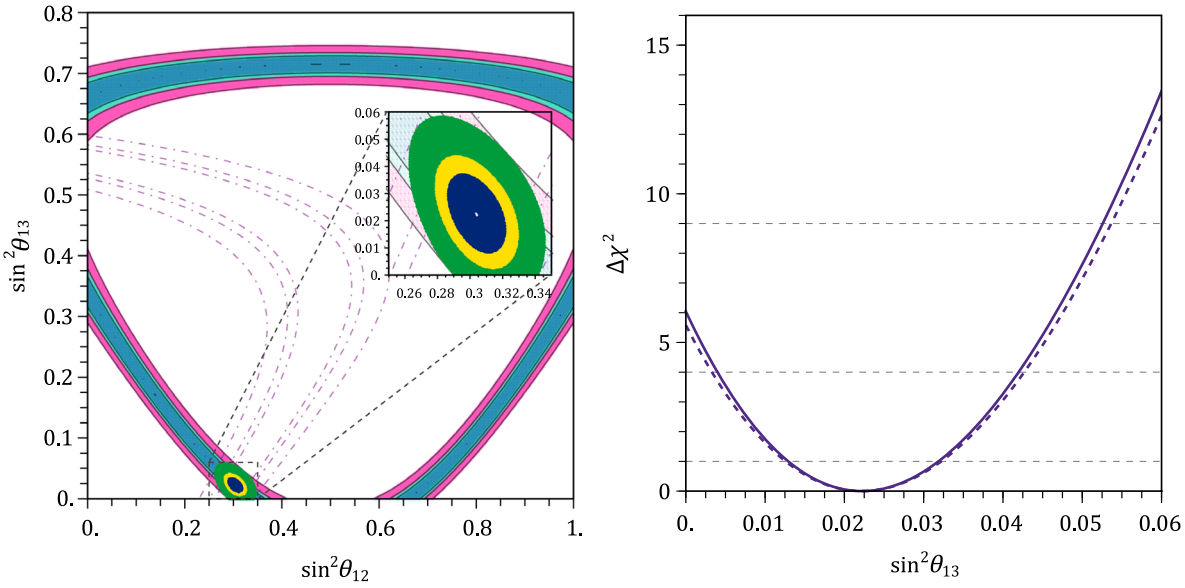

FIG. 1. Right: One-, two- and three-sigma allowed regions of the $\sin^2\theta_{12} \times \sin^2\theta_{13}$ parameter space assuming DARWIN can measure $P_{ee} = 0.552$ at the one percent level, excluding and including (inset figure) external constraints on the neutrino-mixing parameters from other solar experiments. The tiny empty ellipse in the panel indicates the best-fit point. The open regions bound by dashed lines (left-hand panel) represent one-, two- and three-sigma results from current ^{8}B neutrino experiments, as discussed in the text. Left: Solar-only χ^2 as a function of $\sin^2\theta_{13}$, marginalized over $\sin^2\theta_{12}$, assuming 300-ton-years of simulated DARWIN data. The full line corresponds to the assumption of a depleted background, while the dashed line is obtained including the expected natural ^{136}Xe background.

Assuming the three-massive-neutrinos paradigm, this can be converted into a measurement of the relevant mixing parameters. Figure 1 (left) depicts the allowed region of the $\sin^2\theta_{12} \times \sin^2\theta_{13}$ parameter space assuming DARWIN can measure P_{ee} for pp-neutrinos at the 1% level, and assuming the best-fit value is $P_{ee} = 0.552$. There is very strong degeneracy between different values of $\sin^2\theta_{12}$ and $\sin^2\theta_{13}$, for obvious reasons. The degeneracies can be lifted by including constraints from other neutrino experiments.

It is interesting to investigate how well one can constrain neutrino-mixing parameters using only solar-neutrino data. In order to estimate that, we add to the hypothetical pp-neutrino measurement from DARWIN current information from ^{8}B neutrinos, mostly from the Super-Kamiokande and SNO experiments, see [16,17] and references therein. These provide the strongest constraints on $\sin^2\theta_{12}$. Here, we address this in a simplified but accurate way [18], postulating that ^{8}B experiments measure

$$(P_{ee})_{^8\mathrm{B,average}} = (1 - |U_{e3}|^2)[0.9|U_{e2}|^2 + 0.1|U_{e1}|^2] + |U_{e3}|^4, \tag{3.6}$$

with 4% accuracy, consistent with the current uncertainty on $\sin^2\theta_{12}$, mostly constrained by high-energy solar neutrino data. $(1 - |U_{e3}|^2) \times 0.9$ (or $(1 - |U_{e3}|^2) \times 0.1$) is the average probability that a ^{8}B neutrino arrives at the surface of the Earth as a ν_2 (or a ν_1). When the ^{8}B data are treated as outlined above, they translate into the open regions bound by dot-dashed lines in Fig. 1 (left). Strong matter effects lead to the boomerang-shaped allowed region of the parameter space and restrict the parameter space to values of $\sin^2\theta_{12} \lesssim 0.5$. The results of the joint pp–^{8}B analysis are depicted in Fig. 1 (inset figure). All degeneracies present in the pp-neutrino data are lifted and one is constrained to small values of $\sin^2\theta_{13}$ and $\sin^2\theta_{12} < 0.5$.

The combined ^{8}B and DARWIN data can rule out $\sin^2\theta_{13} = 0$ with some precision. This is important; it implies that a hypothetical DARWIN measurement of the pp-neutrino flux, combined with the current ^{8}B solar neutrino data, can measure $\sin^2\theta_{13}$ in a way that is independent from all nonsolar measurements. The marginalized χ^2 as a function of $\sin^2\theta_{13}$ is depicted in Fig. 1 (right), for 300 ton-years of simulated DARWIN data and the current ^{8}B solar neutrino data. On average, if the pp-neutrino flux can be measured at the percent level, we expect to measure $\sin^2\theta_{13}$ at the 35% level and rule out $\sin^2\theta_{13} = 0$ at almost the three-sigma level. Here we consider the two scenarios outlined earlier, one with natural xenon (dashed line), the other with ^{136}Xe-depleted xenon (solid line).

The precision on $\sin^2\theta_{13}$ obtained above is not comparable to that of the current measurement of $\sin^2\theta_{13}$, Eq. (3.3). However, these measurements are qualitatively different. The most precise measurements of $\sin^2\theta_{13}$ come from reactor antineutrino experiments and a baseline of order 1 km [19–21]. The estimate discussed above is a "solar only" measurement, i.e., it exclusively makes use of measurements of neutrinos (and not antineutrinos) produced

in the Sun. Current measurements of $\sin^2\theta_{13}$ that make use of neutrinos (as opposed to antineutrinos), from T2K and NOvA, are much less precise (at the 50%, see [22,23]). Looking further into the future, the DUNE experiment, for example, is expected to independently measure the "neutrino-only" value of $\sin^2\theta_{13}$ at the 20% level [24] (or worse, depending on the assumptions made in the analysis).

IV. BEYOND THE THREE-MASSIVE-NEUTRINOS PARADIGM

The fact that the pp-neutrino flux can be computed with great precision, combined with the sub-MeV pp-neutrino energies, allows a high-statistics measurement of the pp-neutrino flux to meaningfully search for phenomena beyond the three-massive-neutrinos paradigm. Here we concentrate on testing the hypothesis that the neutrinos produced in the Sun have a nonzero probability of behaving as "sterile neutrinos" ν_s, characterized by their lack of participation in charged-current and neutral-current weak interactions.

We first discuss, in Sec. IV A, the case where the oscillation probabilities are energy-independent for the energies of interest, as in the case of the three-massive-neutrinos paradigm discussed in Sec. III. In particular, we test the hypothesis that $P_{ee} + P_{ea} = 1$ for pp-neutrinos. Then, in Sec. IV B, we compute DARWIN's ability to constrain the hypothesis that there is a fourth neutrino ν_4 and that its mass is quasidegenerate with m_1.

A. Model-independent considerations

As discussed in Sec. II, we are interested in the shape and normalization of the electron recoil-energy spectrum from neutrino–electron elastic scattering. The differential cross-section for ν_e and ν_a scattering are different, both in normalization and shape and hence, in principle, one can obtain independent information on both P_{ee} and P_{ea}.

We simulate and analyze 300 ton-years of DARWIN pp-data, as discussed in Sec. II, and attempt to measure P_{ee} and P_{ea} independently. To illustrate the dependence of the electron recoil spectrum on these probabilities, we present in Fig. 2 the event rate for $(P_{ee}, P_{ea}) = (0.55, 0.45)$ (purple), (0.45,0.8) (dashed cyan), and (0.62,0.10) (dotted orange), together with the ^{124}Xe background lines (gray lines), "natural" ^{136}Xe background (gold) and "depleted" ^{136}Xe background (gold dashed). The crucial characteristic that allows for the independent determination of P_{ee} and P_{ea} corresponds to the different behavior of cross sections for ν_e and $\nu_{\mu,\tau}$ scattering with electrons, which lead to distinct recoil spectra, specially at low energies. In the case where $P_{ea} > P_{ee}$, without assuming $P_{ee} + P_{ea} = 1$, the contribution of the nonelectron neutrinos to the final spectrum is important, leading to a significant modification at low recoil energies with respect to the standard case. On the contrary, when $P_{ea} < P_{ee}$, the event rate is closer to the standard one at low energies, but differs more significantly

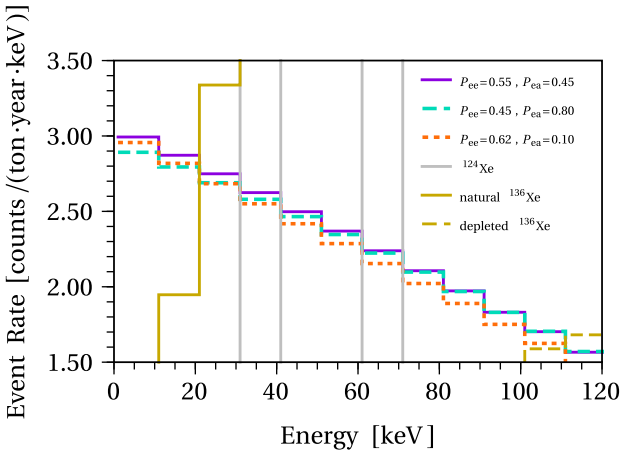

FIG. 2. Electron recoil spectrum for three different cases of $(P_{ee}, P_{ea}) = (0.55, 0.45)$ (purple), (0.45,0.8) (dashed cyan), and (0.62,0.10) (dotted orange). We also present the backgrounds considered in our analysis, ^{124}Xe background lines (gray), "natural" ^{136}Xe background (gold) and "depleted" ^{136}Xe background (gold dashed).

at larger recoil energies. Thus, we observe that a detailed analysis of the recoil spectrum could demonstrate the departure from the standard oscillation scenario.

The results of our analysis are depicted in Fig. 3 (left) for both the natural xenon (dashed) and the ^{136}Xe-depleted (solid) hypotheses. Strong departures from $P_{ee} + P_{ea} = 1$ are allowed and the "natural" data are not capable of ruling out $P_{ea} = 0$ at the three-sigma confidence level. The "depleted" data can rule out $P_{ea} = 0$ at the five-sigma confidence level. For both scenarios, one can constrain the departure of $P_{ee} + P_{ea}$ from one, which we interpret as the oscillation probability into sterile neutrinos $P_{es} \equiv 1 - P_{ee} - P_{ea}$. The colorful diagonal lines in Fig. 3 (left) correspond to different constant values of P_{es}. Figure 3 (right) depicts χ^2 as a function of P_{es}, marginalized over P_{ee} and restricting P_{es} to non-negative values for both scenarios. If DARWIN data are consistent with the three-active-neutrinos paradigm, they will be capable of constraining $P_{es} < 0.35$ at the two-sigma confidence level even if DARWIN is filled with natural xenon.

B. Fourth-neutrino hypothesis

We explore in more detail the scenario where there is one extra neutrino mass-eigenstate ν_4 with mass m_4. In this case, the interaction eigenstates are, including ν_s, related to the four mass-eigenstates via a 4×4 unitary matrix $U_{\alpha i}$, $\alpha = e, \mu, \tau, s$, $i = 1, 2, 3, 4$. We will concentrate on the scenario where, among the four U_{si}, only U_{s1} and U_{s4} are potentially nonzero.[3] In this case, we can parameterize the

[3]It is easy to generalize this analysis assuming that only one of the U_{sj}, $j = 1, 2, 3$, and U_{s4} are potentially nonzero. We spell this out in the Appendix.

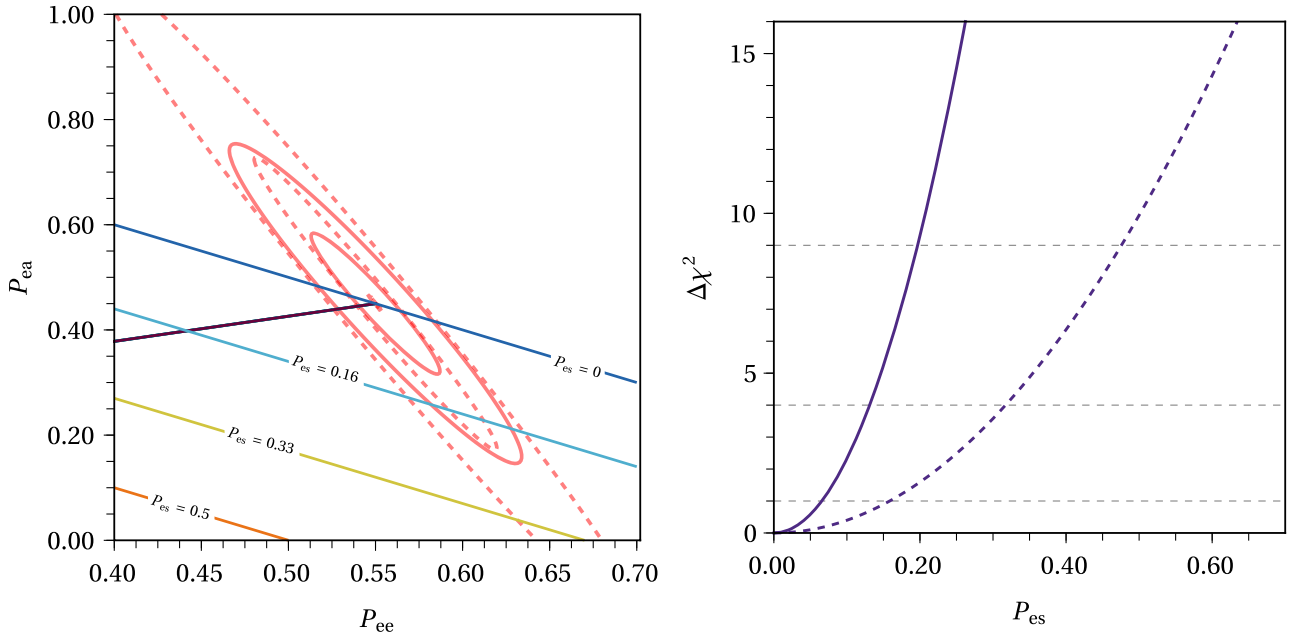

FIG. 3. Left: One- and three-sigma allowed region of the $P_{ee} \times P_{ea}$-plane, for 300 ton-years of simulated DARWIN data. The diagonal lines correspond to constant $P_{es} \equiv 1 - P_{ee} - P_{ea}$ values. The burgundy line segment with positive slope corresponds to the values of $(P_{ee}, P_{ea}) = (0.55 - 0.23\sin^2 2\theta_{14}, 0.45 - 0.11\sin^2 2\theta_{14})$ obtained by varying $\sin^2 2\theta_{14} \in [0, 1]$, cf. Eqs. (4.9). Right: Marginalized χ^2 as a function of P_{es}. The full line correspond to the assumption of a depleted background, while the dashed line is obtained considering no cuts in the ^{136}Xe background.

$|U_{ei}|^2$ entries of the mixing matrix using three mixing angles θ_{12}, θ_{13}, θ_{14}. Eqs. (3.2) are still valid, along with

$$|U_{e1}|^2 = \cos^2\theta_{12}\cos^2\theta_{13}\cos^2\theta_{14},$$
$$|U_{e4}|^2 = \cos^2\theta_{12}\cos^2\theta_{13}\sin^2\theta_{14}. \tag{4.1}$$

It is easy to check that $\sum_{i=1}^{4} |U_{ei}|^2 = 1$. The nonzero "sterile" entries of the mixing matrix are

$$|U_{s1}|^2 = \sin^2\theta_{14}, \qquad |U_{s4}|^2 = \cos^2\theta_{14}. \tag{4.2}$$

Given the quasi-two-flavors nature of these solar neutrino oscillations, to be discussed momentarily, the entire physical parameter space is spanned by either fixing $\Delta m^2_{41} > 0$ and allowing $\sin^2\theta_{14} \in [0, 1]$ or allowing both signs for Δm^2_{41} and restricting $\sin^2\theta_{14} \in [0, 0.5]$ in such a way that ν_4 is always "mostly sterile." Here, the former convention—to fix the sign of $\Delta m^2_{41} > 0$—is most convenient. With this choice, when $\sin^2\theta_{14} \in [0, 0.5]$, the heaviest of the two quasidegenerate states (i.e., ν_4) is mostly sterile, when $\sin^2\theta_{14} \in [0.5, 1]$, the lightest among the two quasidegenerate states (i.e., ν_1) is mostly sterile. For historical reasons, we will refer to $\sin^2\theta_{14} \in [0, 0.5]$ as the light side of the parameter space and $\sin^2\theta_{14} \in [0.5, 1]$ as the dark side [25].

Before proceeding, we want to highlight that while the scenario we are considering here is a subset of the most general three-active-one-sterile neutrino scenario, it can be realized in concrete models. For example, we can add to the standard model particle content a sterile fermion ν_s with mass m_s along with a new "neutrino-portal" interaction between ν_s and ν_{1a}, where ν_{1a} (a for active) is one of the eigenstates, with eigenvalue m_{1a}, of the active neutrino mass matrix. Including the new interaction (proportional to some mass parameter $m_{\rm mix}$), the eigenstates of the 4×4 neutrino mass matrix are the ones described above. In this case, m_1, m_4, θ_{14} are functions of m_{1a}, m_s, $m_{\rm mix}$. A natural realization of this scenario is the one that leads to so-called pseudo-Dirac neutrinos (see, for example, [9,10] for more details), where $m_{1a}, m_s \ll m_{\rm mix}$. In this case, we expect $\theta_{14} \sim \pi/4$ and $m_1 \sim m_4$.

We are interested in the hypothesis that $\Delta m^2_{41} \ll \Delta m^2_{21}$ and outside the reach of all current neutrino experiments. In this case, the current neutrino oscillation data constrain the oscillation parameters Δm^2_{21}, Δm^2_{31}, $\sin^2\theta_{12}$, and $\sin^2\theta_{13}$ exactly as in the three-massive-neutrinos paradigm. Furthermore, building on the discussion in Sec. III, it is easy to conclude that the oscillation probabilities of interest $P_{e\alpha}$, $\alpha = e$, a, s, are only functions of $\sin^2\theta_{12}$, $\sin^2\theta_{13}$, $\sin^2\theta_{14}$, and Δm^2_{41}. Further taking advantage of the fact that $|\Delta m^2_{21}|/(2E), |\Delta m^2_{31}|/(2E) \gg V_\odot$, it is straightforward to compute

$$P_{ee} = |U_{e2}|^4 + |U_{e3}|^4 + (1 - |U_{e2}|^2 - |U_{e3}|^2)^2 P^{2f}_{ee}(\Delta m^2_{41}, \sin^2\theta_{14}, V^{\rm eff}), \tag{4.3}$$

$$P_{es} = (1 - |U_{e2}|^2 - |U_{e3}|^2)(1 - P_{ee}^{2f}(\Delta m_{41}^2, \sin^2\theta_{14}, V^{\text{eff}})), \tag{4.4}$$

$$P_{ea} = 1 - P_{ee} - P_{es}, \tag{4.5}$$

where P_{ee}^{2f} is the survival probability obtained in the scenario where there are only two flavors, ν_e^{2f} and ν_s^{2f}, characterized by the mass-squared difference Δm_{41}^2 and the mixing angle θ_{14}, defined via $\nu_e^{2f} = \cos\theta_{14}\nu_1 + \sin\theta_{14}\nu_4$. Inside P_{ee}^{2f}, the matter potential is replaced by an effective matter potential V^{eff}. It takes into account the neutral-current contribution to the matter potential $V_{NC} = -\sqrt{2}/2 G_F N_n$, where N_n is the neutron number density in the medium, while the charged-current contribution is rescaled by $(1 - |U_{e2}|^2 - |U_{e3}|^2) = \cos^2\theta_{13}\cos^2\theta_{12}$:

$$V^{\text{eff}} = \sqrt{2} G_F \left(N_e \cos^2\theta_{13}\cos^2\theta_{12} - \frac{1}{2} N_n \right). \tag{4.6}$$

In the sun, the position-dependency of the electron and neutron number densities are slightly different [2].[4] In the sun's core, N_n is around 50% of N_e and V^{eff} is slightly less than one half of the standard matter potential.

Equation (4.3) allows us to estimate, in very general terms, the impact of the sterile neutrinos. For $P_{ee}^{2f} = 1$, we recover the three-active-neutrinos result, $P_{ee} = \cos^4\theta_{12}\cos^4\theta_{13} + \sin^4\theta_{12}\cos^4\theta_{13} + \sin^4\theta_{13}$, Eq. (3.4). On the other hand, for $P_{ee}^{2f} = 0$, $P_{ee} = \sin^4\theta_{12}\cos^4\theta_{13} + \sin^4\theta_{13}$ such that, given the current knowledge of oscillation parameters,

$$P_{ee} \in [0.09, 0.55]. \tag{4.7}$$

P_{es} values, on the other hand, are allowed to be as small as zero and as large as 0.68.

In Sec. IV A, we discussed that, very generically, DARWIN can rule out $P_{es} < 0.35$ at the two-sigma level. The situation here is more constrained as P_{ee}, P_{ea}, P_{es} are not only required to add up to one but depend on the same oscillation parameters. We proceed to discuss the sensitivity of DARWIN to the new oscillation parameters Δm_{41}^2, $\sin^2\theta_{14}$ by taking advantage of the fact that the properties of P_{ee}^{2f} are well known (see, for example, [26]).

1. Large Δm_{41}^2: Matter effects are irrelevant

For large-enough values of Δm_{41}^2, P_{ee}^{2f} is well approximated by averaged-out vacuum oscillations:

[4]There are relatively more neutrons in the center of the sun relative to its edges. This is due to the fact that most of the solar helium is concentrated in the core.

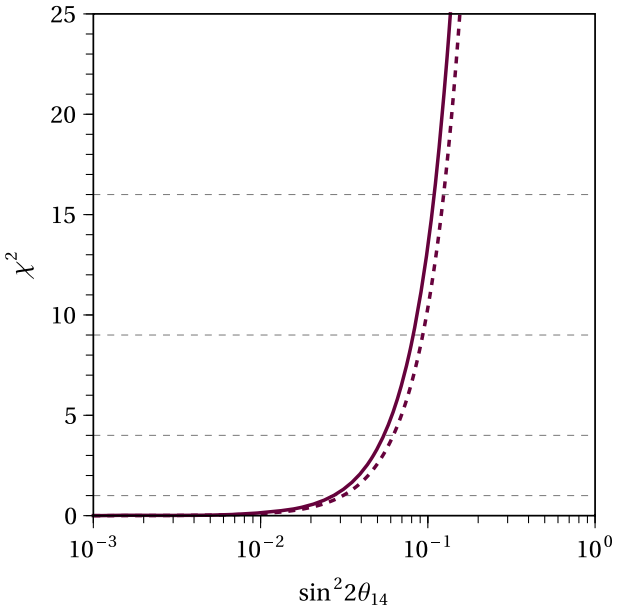

FIG. 4. χ^2 as a function of $\sin^2\theta_{14}$ for 300 ton-years of simulated DARWIN data, in the regime when matter effects are not significant and the new oscillatory effects driven by Δm_{41}^2 average out. The full line corresponds to the assumption of a depleted background, while the dashed line is obtained considering no cuts in the ^{136}Xe background.

$$P_{ee}^{2f,\text{ave}} = 1 - \frac{1}{2}\sin^2 2\theta_{14}. \tag{4.8}$$

This occurs, keeping in mind we are interested in energies below 420 keV, for $\Delta m_{41}^2 \gtrsim 10^{-5}$ eV^2, when the solar matter effects can be ignored. In this case,

$$\begin{aligned} P_{ee} &= 0.55 - 0.23\sin^2 2\theta_{14}, \\ P_{es} &= 0.34\sin^2 2\theta_{14}, \\ P_{ea} &= 0.45 - 0.11\sin^2 2\theta_{14}. \end{aligned} \tag{4.9}$$

Here, it is impossible to distinguish the light from the dark side of the parameter space since the oscillation probabilities are invariant under $\sin^2\theta_{14} \leftrightarrow 1 - \sin^2\theta_{14}$. Varying $\sin^2 2\theta_{14} \in [0, 1]$, Eqs. (4.9) define a line segment in the $P_{ee} \times P_{ea}$-plane, depicted in Fig. 3 (left)—burgundy line with positive slope—keeping in mind the segment extends to P_{ee} values below 0.4. Figure 4 depicts χ^2 as a function of $\sin^2\theta_{14}$ in the regime where Eqs. (4.9) are a good approximation, for 300 ton-years of simulated DARWIN data, for both the natural (dashed) and ^{136}Xe-depleted (solid) scenarios. In this analysis, and in the upcoming analyses discussed in this subsection, we assume that $\sin^2\theta_{13}$ and $\sin^2\theta_{12}$ are known with infinite precision. This is, currently, a good approximation for $\sin^2\theta_{13}$ and will be a good approximation for $\sin^2\theta_{12}$ once data from the JUNO experiment is analyzed [27]. Similar results were

recently presented and discussed in [28]. Where are assumptions agree, the estimated sensitivity also agrees.

2. Intermediate Δm^2_{41}: Strong matter effects, adiabatic regime

For intermediate values of Δm^2_{41}, P^{2f}_{ee} is well described by the strong MSW effect in the adiabatic regime. In this case, for a range of energies,

$$P^{2f,\text{adiabatic}}_{ee} = \sin^2\theta_{14}. \tag{4.10}$$

For pp-neutrinos, this occurs for, very roughly, $\sin^2\theta_{14} \gtrsim 10^{-3}$ and $10^{-9} \lesssim \Delta m^2_{41}/(\text{eV}^2) \lesssim 10^{-6}$. Under these conditions,

$$\begin{aligned} P_{ee} &= 0.09 + 0.46\sin^2\theta_{14}, \\ P_{es} &= 0.68 - 0.68\sin^2\theta_{14}, \\ P_{ea} &= 0.27 + 0.22\sin^2\theta_{14}. \end{aligned} \tag{4.11}$$

Here, oscillation probabilities are very different in the light and dark sides. In particular, in the light side of the parameter space P_{ee} (P_{es}) is small (large) and increases (decreases) linearly with $\sin^2\theta_{14}$. If DARWIN data are consistent with three-active neutrinos, in this region of parameter space, small values of $\sin^2\theta_{14}$ will be excluded while large values of $\sin^2\theta_{14}$ are allowed.

3. Small Δm^2_{41}: Very strong matter effects, nonadiabatic regime

For small-enough values of Δm^2_{41}, P^{2f}_{ee} is well described by the strong MSW effect in the very nonadiabatic regime and turns out to be well approximated by vacuum oscillations,

$$P^{2f,\text{ave}}_{ee} = 1 - \sin^2 2\theta_{14}\sin^2\left(\frac{\Delta m^2_{41}L}{4E}\right). \tag{4.12}$$

This occurs, for pp-neutrinos, for $\Delta m^2_{41} \lesssim 10^{-9}$ eV^2. In this case,

$$\begin{aligned} P_{ee} &= 0.55 - 0.46\sin^2 2\theta_{14}\sin^2\left(\frac{\Delta m^2_{41}L}{4E}\right), \\ P_{es} &= 0.68\sin^2 2\theta_{14}\sin^2\left(\frac{\Delta m^2_{41}L}{4E}\right), \\ P_{ea} &= 0.45 - 0.22\sin^2 2\theta_{14}\sin^2\left(\frac{\Delta m^2_{41}L}{4E}\right). \end{aligned} \tag{4.13}$$

Here, again, it is impossible to distinguish the light from the dark side of the parameter space. Given the average Earth–Sun distance $L = 1.5 \times 10^{12}$ m, the oscillation phase is

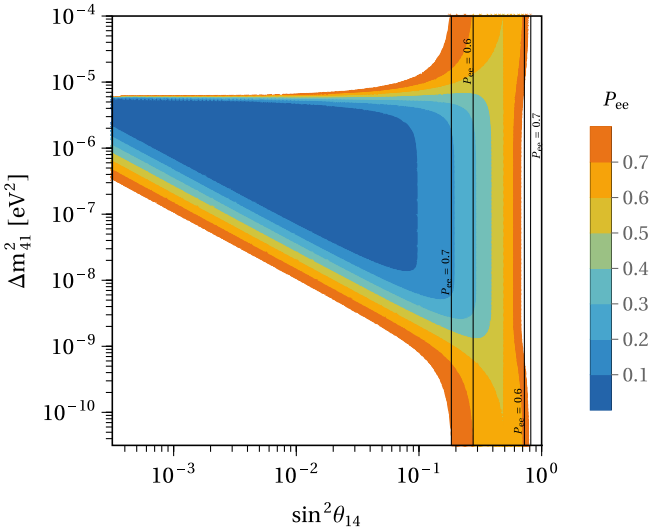

FIG. 5. Contours of constant P_{ee} in the $\Delta m^2_{41} \times \sin^2\theta_{14}$-plane for $E = 300$ keV. $\sin^2\theta_{12}$, $\sin^2\theta_{13}$ are fixed to their best-fit values, Eq. (3.3). The vertical lines correspond to constant values of the averaged-out vacuum oscillation probability for $P_{ee} = 0.6$, 0.7.

$$\frac{\Delta m^2_{41}L}{4E} = 4.8\left(\frac{\Delta m^2_{41}}{10^{-12}\text{ eV}^2}\right)\left(\frac{400\text{ keV}}{E}\right), \tag{4.14}$$

so we expect the vacuum oscillations to average out for $\Delta m^2_{41} \gtrsim 10^{-11}$ eV^2. This means that, for $10^{-11} \lesssim \Delta m^2_{41}/(\text{eV}^2) \lesssim 10^{-9}$, the oscillation probabilities are well described by Eqs. (4.9).

Figure 5 depicts contours of constant P_{ee} in the $\Delta m^2_{41} \times \sin^2\theta_{14}$-plane for $E_\nu = 300$ keV and allows one to identify the different regimes discussed here. The other parameters are fixed to their current best-fit values, Eq. (3.3). We describe the assumed matter potential for active and sterile neutrinos in Appendix B. Under these circumstances, P^{2f}_{ee} can be computed exactly [29]. For simplified pedagogical discussions see, for example, [26,30]. We assume all solar neutrinos are produced in the exact center of the Sun; we explicitly verified that the results we get are very similar to the results we would have obtained by integrating over the region where pp-neutrinos are produced. The region where matter effects are strong and the adiabatic condition holds correspond to the vertical sides of the constant P_{ee} regions that form quasitriangles. The "return" to vacuum oscillations at low and high values of Δm^2_{41} is highlighted by the vertical, dark lines, which correspond to constant values of the averaged-out vacuum oscillation probability. For a detailed discussion of the boundary between the adiabatic and nonadiabatic transition, including L dependent effects, see [31].

4. Sensitivity

We simulate 300 ton-years of DARWIN data consistent with the three-massive-neutrinos paradigm and assuming

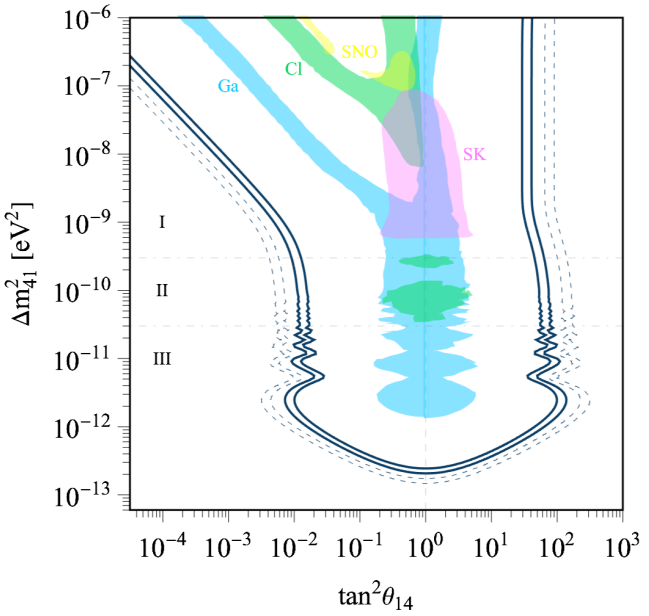

FIG. 6. Two- and three-sigma sensitivity of 300 ton-years of DARWIN data to a light sterile neutrino in the $\Delta m^2_{41} \times \tan^2\theta_{14}$–plane. The dashed lines correspond to the assumption of a depleted ^{136}Xe background, while the full lines are for the full case. The parallel inner and outer contours correspond to different assumptions about the precision with which the pp-flux is known.The colored regions correspond to current limits from Ga (blue), Cl (green), SuperK (pink) and SNO (Yellow) experiments. The regions separated by the gray dot-dashed lines indicate approximately where some of the different regimes discussed in the text apply: (I) strong adiabatic MSW regime; (II) averaged-out vacuum oscillations; (III) long-wavelength vacuum oscillations.

the true values of $\sin^2\theta_{12}$ and $\sin^2\theta_{13}$ are the ones in Eq. (3.3). We restrict our discussion to values of $\Delta m^2_{41} < 10^{-6}$ eV^2. Larger values are constrained by measurements of higher-energy solar neutrinos; these constraints have been explored in [32,33], along with a detailed discussion of the oscillation probabilities. The expressions we derive here are contained in the analyses of [32,33] if one explores them in the appropriate regime.

Figure 6 depicts the region of the $\tan^2\theta \times \Delta m^2_{41}$–plane inside of which 300 ton-years of DARWIN data is sensitive, at the 90% confidence level, to the fourth neutrino for both the natural-xenon scenario (dashed line) and the depleted-^{136}Xe scenario (solid). We include the current limits from Gallium (blue), Chlorine (green), SuperK (pink), and SNO (yellow) experiments, taken from [34]. We indicate with the gray dot-dashed horizontal lines where some of the different oscillation regimes described above approximately apply: (I) strong adiabatic MSW regime; (II) averaged-out vacuum oscillations; (III) long-wavelength vacuum oscillations. On a log-scale, the contour is symmetric relative to $\tan^2\theta_{14} = 1$ when one cannot distinguish the light from the dark side of the parameter space [25], a feature one readily observes, as advertised, for small values of Δm^2_{41}. The impact of nontrivial matter effects is also readily observable. For larger values of the Δm^2_{41}, the sensitivity to small mixing angles is expected to "shut-off" quickly—see Fig. 5—and would return to values similar to those around $\Delta m^2_{41} \sim 10^{-10}$ eV^2, minus the tiny wiggles.

The sensitivity depicted in Fig. 6 includes the marginalization over the normalization of the backgrounds discussed in Sec. II. We also investigated the impact of the current uncertainties in the standard ν-mixing parameters [15]. The most relevant for our analysis is $\sin^2\theta_{12}$ and we find that its uncertainty has a negligible impact in the sensitivity to the sterile neutrinos. Throughout, we also assumed that the pp-neutrino flux is known with infinite precision. In order to investigate the impact of this approximation, we also included a prior on the pp-flux, along with a 0.6% normalization uncertainty. The impact is depicted in Fig. 6. The "outside" sensitivity regions for both natural or ^{136}Xe-depleted xenon correspond to infinite precision on the normalization of the pp-flux while the "inside" sensitivity regions correspond to the 0.6% uncertainty. The impact of not predicting the pp-flux with infinite precision is relatively small but observable.

5. *Sensitivity to pseudo-Dirac neutrinos*

The low energies of the pp-neutrinos combined with the long Earth–Sun distance render DARWIN a specially powerful probe of the hypothesis that neutrinos are pseudo-Dirac fermions. This is the hypothesis that there are right-handed neutrinos coupled to the left-handed lepton doublets and the Higgs doublet via a tiny Yukawa coupling y and that lepton number is only slightly violated. In these scenarios, each of the neutrino mass eigenstates is "split" into two quasidegenerate Majorana fermions, each a 50–50 mixture of an active neutrino (from the lepton doublet) and a sterile neutrino (the right-handed neutrino). The mass splitting is small enough that, for most applications, the two quasidegenerate states act as one Dirac fermion. Pseudo-Dirac neutrinos reveal themselves via active–sterile oscillations associated with very large mixing and very small mass-squared differences.

In the language introduced here, a pseudo-Dirac neutrino corresponds to $\sin^2 2\theta_{14} = 1$ (maximal mixing) and the small mass-squared difference leads to a nonzero $\Delta m^2_{41} = 4\epsilon m_1$ where $m_1 \pm \epsilon$ are the masses of the two quasidegenerate states (here ν_1 and ν_4), m_1 is the Dirac mass, proportional to the neutrino Yukawa coupling, and ϵ characterizes the strength of the lepton-number violating physics. Figure 7 depicts χ^2 as a function of Δm^2_{41} for $\sin^2 2\theta_{14} = 1$ associated with 300 ton-years of simulated DARWIN data for both the natural xenon (dashed) and the ^{136}Xe-depleted (solid) scenarios, assuming the data are consistent with no new neutrino states. Current solar

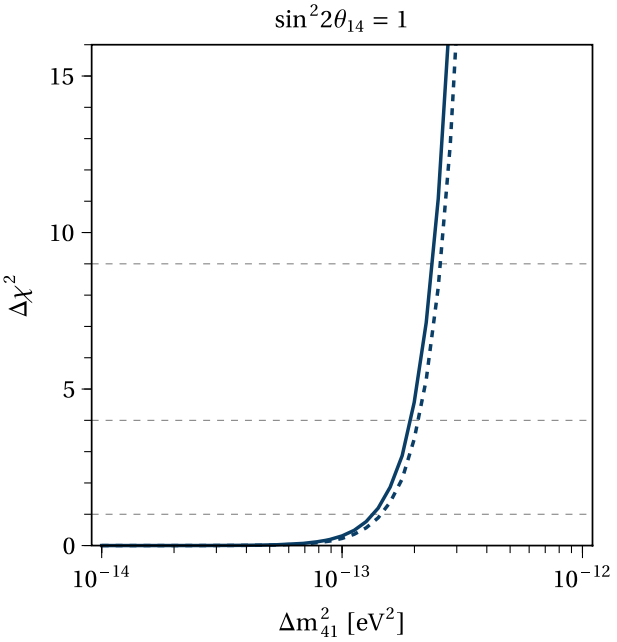

FIG. 7. Darwin sensitivity to the quadratic mass difference Δm^2_{41} in the case of maximal mixing, $\sin^2\theta_{14} = 0.5$. The full line correspond to the assumption of a depleted background, while the dashed line is obtained considering no cuts in the ^{136}Xe background.

neutrino data exclude Δm^2_{41} values larger than 10^{-12} eV^2 [9,10] so DARWIN can extend the sensitivity to Δm^2_{41} (and hence, the new, lepton-number violating parameter ϵ) by an order of magnitude.

V. CONCLUDING REMARKS

Next-generation WIMP-dark-matter-search experiments will be exposed to a large-enough flux of solar neutrinos that neutrino-mediated events are unavoidable. The DARWIN collaboration recently argued that DARWIN can collect a large, useful sample of solar pp-neutrinos, detected via elastic neutrino–electron scattering [1], and measure the survival probability of pp-neutrinos with subpercent precision. Here we explored the physics potential of such a sample in more detail, addressing other concrete neutrino-physics questions and exploring whether one can also extract information from a precise measurement of the shape of the differential pp-neutrino flux.

We estimate that, with 300 ton-years of data, DARWIN can not only measure the survival probability of pp-neutrinos with subpercent precision but also determine, with the help of current solar neutrino data, the value of $\sin^2\theta_{13}$, with the potential to exclude $\sin^2\theta_{13} = 0$ close to the three sigma level. Such a pp-neutrino sample would allow one to perform a "neutrinos-only" (and solar-neutrinos-only) measurement of $\sin^2\theta_{13}$ and $\sin^2\theta_{12}$. Such a measurement can be compared with, for example, reactor-based "antineutrinos-only" measurements of the same mixing parameters and allow for nontrivial tests of the *CPT*-theorem and other new physics scenarios. In our analysis, we include the two most important sources of background as described by the DARWIN collaboration—the ^{124}Xe and ^{136}Xe backgrounds—and we have considered a 0.6% normalization uncertainty on the prediction of the pp flux.

DARWIN can also test the hypothesis that pp-neutrinos are oscillating into a combination of active and sterile neutrinos. We estimate that DARWIN data can exclude the hypothesis that the pp-neutrinos are "disappearing" in an energy independent way—assuming their data are consistent with the three-active-neutrinos paradigm—especially if the experiment manages to fill their detector with ^{136}Xe-depleted xenon.

We explored in some detail how well DARWIN can constrain the existence of a new neutrino mass-eigenstate ν_4 (mass m_4) that is quasidegenerate and mixes with ν_1, i.e., $\Delta m^2_{41} \ll \Delta m^2_{21}$, $U_{s1}, U_{s4} \neq 0$, $U_{s2} = U_{s3} = 0$. Our estimated sensitivity is depicted in Fig. 6. It supersedes that of all current and near-future searches for new, very light neutrinos. In particular, DARWIN can test the hypothesis that ν_1 is a pseudo-Dirac fermion as long as the induced mass-squared difference is larger than 10^{-13} eV^2. This is one order of magnitude more sensitive than existing constraints [9,10].

Throughout, we allowed for the hypotheses that DARWIN is filled with natural xenon or ^{136}Xe-depleted xenon. We find that while the sensitivity of the experiment with natural xenon is outstanding, a ^{136}Xe-depleted setup is significantly more sensitive when it comes to the measurements and searches discussed here. In our discussions, we did not include time-dependent effects (the seasonal and day-night effects). These can impact the sensitivity to new neutrino states within a subset of the parameter space explored here. They would not significantly modify the results discussed here but provide extra handles on the new physics.

ACKNOWLEDGMENTS

We thank Pedro Machado for discussions of potential uses of DARWIN data for neutrino physics. This work was supported in part by the U.S. Department of Energy (DOE) Grant No. de-sc0010143 and in part by the NSF Grant No. PHY-1630782. The document was prepared using the resources of the Fermi National Accelerator Laboratory (Fermilab), a DOE, Office of Science, HEP User Facility. Fermilab is managed by Fermi Research Alliance, LLC (FRA), acting under Contract No. DE-AC02-07CH11359. This material is based upon work supported by the NSF Grant No. AST-1757792, a Research Experience for Undergraduates grant awarded to the Center for Interdisciplinary Exploration and Research in Astrophysics (CIERA) at Northwestern University. I. M. S. is supported by the Faculty of Arts and Sciences of Harvard University.

APPENDIX A: OTHER FOURTH-NEUTRINO SCENARIOS

We restricted our fourth-neutrino analyses to one new neutrino mass-eigenstate ν_4 and allowed for only "1–4" sterile mixing, i.e., $U_{s1} = \sin\theta_{14}$, $U_{s4} = \cos\theta_{14}$ while $U_{s2} = U_{s3} = 0$. Here we discuss some simple generalizations.

The case of one new neutrino mass-eigenstate ν_5 that is quasidegenerate with ν_2 and only "2–5" sterile mixing would also be parametrized by a mass-squared difference Δm^2_{52} (positive-definite), assumed to be much smaller than Δm^2_{21}, Δm^2_{51} and $|\Delta m^2_{53}|$, and one mixing angle θ_{25}:

$$U^2_{e1} = \cos^2\theta_{12}\cos^2\theta_{13}, \qquad U^2_{e2} = \sin^2\theta_{12}\cos^2\theta_{13}\cos^2\theta_{25}, \qquad U^2_{e3} = \sin^2\theta_{13}, \qquad U^2_{e5} = \sin^2\theta_{12}\cos^2\theta_{13}\sin^2\theta_{25}, \tag{A1}$$

$$U^2_{s1} = 0, \qquad U^2_{s2} = \sin^2\theta_{25}, \qquad U^2_{s3} = 0, \qquad U^2_{s5} = \cos^2\theta_{25}. \tag{A2}$$

Similar to Eq. (4.3), and the equivalent expressions for P_{ea} and P_{es}, here

$$P_{ee} = |U_{e1}|^4 + |U_{e3}|^4 + (1 - |U_{e1}|^2 - |U_{e3}|^2)^2 P^{2f}_{ee}(\Delta m^2_{52}, \sin^2\theta_{25}, V^{\rm eff}_{25}), \tag{A3}$$

$$P_{es} = (1 - |U_{e1}|^2 - |U_{e3}|^2)(1 - P^{2f}_{ee}(\Delta m^2_{52}, \sin^2\theta_{25}, V^{\rm eff}_{25})), \tag{A4}$$

$$P_{ea} = 1 - P_{ee} - P_{es}, \tag{A5}$$

where P^{2f}_{ee} is the survival probability obtained in the scenario where there are only two flavors, ν^{2f}_e and ν^{2f}_s, characterized by the mass-squared difference Δm^2_{52} and the mixing angle θ_{25}, defined via $\nu^{2f}_e = \cos\theta_{25}\nu_2 + \sin\theta_{25}\nu_5$. Here, the effective matter potential is

$$V^{\rm eff}_{25} = \sqrt{2} G_F \left(N_e \cos^2\theta_{13}\sin^2\theta_{12} - \frac{1}{2} N_n \right). \tag{A6}$$

On the other hand, the case of one new neutrino mass-eigenstate ν_6 that is quasidegenerate with ν_3 and only "3–6" sterile mixing would also be parametrized by a mass-squared difference Δm^2_{63} (positive-definite), assumed to be much smaller than Δm^2_{21}, $|\Delta m^2_{61}|$ and $|\Delta m^2_{62}|$, and one mixing angle θ_{36}:

$$U^2_{e1} = \cos^2\theta_{12}\cos^2\theta_{13}, \qquad U^2_{e2} = \sin^2\theta_{12}\cos^2\theta_{13}, \qquad U^2_{e3} = \sin^2\theta_{13}\cos^2\theta_{36}, \qquad U^2_{e5} = \sin^2\theta_{13}\sin^2\theta_{36}, \tag{A7}$$

$$U^2_{s1} = 0, \qquad U^2_{s2} = 0, \qquad U^2_{s3} = \sin^2\theta_{36}, \qquad U^2_{s5} = \cos^2\theta_{36}. \tag{A8}$$

Similar to Eq. (4.3), and the equivalent expressions for P_{ea} and P_{es}, here

$$P_{ee} = |U_{e1}|^4 + |U_{e2}|^4 + (1 - |U_{e1}|^2 - |U_{e2}|^2)^2 P^{2f}_{ee}(\Delta m^2_{63}, \sin^2\theta_{36}, V^{\rm eff}_{36}), \tag{A9}$$

$$P_{es} = (1 - |U_{e1}|^2 - |U_{e2}|^2)(1 - P^{2f}_{ee}(\Delta m^2_{63}, \sin^2\theta_{36}, V^{\rm eff}_{36})), \tag{A10}$$

$$P_{ea} = 1 - P_{ee} - P_{es}, \tag{A11}$$

where P^{2f}_{ee} is the survival probability obtained in the scenario where there are only two flavors, ν^{2f}_e and ν^{2f}_s, characterized by the mass-squared difference Δm^2_{63} and the mixing angle θ_{36}, defined via $\nu^{2f}_e = \cos\theta_{36}\nu_3 + \sin\theta_{36}\nu_6$. Here, the effective matter potential is

$$V^{\rm eff}_{36} = \sqrt{2} G_F \left(N_e \sin^2\theta_{13} - \frac{1}{2} N_n \right). \tag{A12}$$

Qualitatively, the three scenarios—1–4, 2–5, 3–6—are identical modulo relabelings of the mixing parameters. Quantitatively, however, there are significant differences. The coefficients of the P^{2f}_{ee} term in Eqs. (4.3), (A3), and (A9) are, respectively, $(\cos^2\theta_{12}\cos^2\theta_{13})^2 \sim 0.5$, $(\sin^2\theta_{12}\cos^2\theta_{13})^2 \sim 0.1$, and $(\sin^2\theta_{13})^2 \sim 0.0005$. These numbers define the maximum deviation of P_{ee} from expectations from the three-massive-neutrinos paradigm,

$P_{ee} \sim 0.55$. Hence, very generically, 1–4 effects can be very strong, as discussed in the text, 2–5 effects are at most of order 20%, and 3–6 effects are at the permille level. On the other hand, the effective potentials are also quantitatively very different. The charged-current contribution to $V_{25}^{\rm eff}$ [Eq. (A6)] is suppressed relative to the neutral-current one by a factor $\sin^2\theta_{12}\cos^2\theta_{13} \sim 0.3$. Since N_n/N_e varies between, roughly, 0.5 and less than 0.1 between the center of the Sun and its edge, $V_{25}^{\rm eff}$ is significantly smaller than $V_\odot$, almost vanishing at the Sun's core, when the charged- and neutral-current contributions, accidentally, almost cancel out one another. $V_{36}^{\rm eff}$ [Eq. (A12)], instead, is solidly dominated by the neutral-current matter potential since the charged-current contribution is suppressed by $\sin^2\theta_{13} \sim 0.02$. Not only is it smaller than $V_\odot$, it has the opposite sign, a fact that qualitatively impact the behavior of P_{ee}^{2f}.

The scenario where all neutrinos are pseudo-Dirac fermions is equivalent to the combination of the 1–4, 2–5, and 3–6 scenarios spelled out above (see, for example, [9]). Note that such a combination is straight forward; the effects of the different contributions simply "add up" without too much interference, as long as the new mass-squared differences are "isolated enough," i.e., the three new mass-squared differences Δm_{41}^2, Δm_{52}^2, and Δm_{63}^2 are much smaller than all other mass-squared differences. For example,

$$P_{ee} = (\cos^2\theta_{12}\cos^2\theta_{13})^2 P_{ee}^{2f}(\Delta m_{41}^2, \sin^2\theta_{14}, V_{14}^{\rm eff}) + (\sin^2\theta_{12}\sin^2\theta_{13})^2 P_{ee}^{2f}(\Delta m_{52}^2 \sin^2\theta_{25}, V_{25}^{\rm eff}) + (\sin^2\theta_{13})^2 P_{ee}^{2f}(\Delta m_{63}^2, \sin^2\theta_{36}, V_{36}^{\rm eff}), \tag{A13}$$

where $V_{14}^{\rm eff}$ is given by Eq. (4.6).

APPENDIX B: SOLAR MATTER POTENTIAL FOR ACTIVE AND STERILE NEUTRINOS

We assume the matter potential is spherically symmetric and drops exponentially, $V^{\rm eff} \propto e^{-r/r_0^s}$. We fit information from the prediction of the B16-GS98 solar model [4] and obtain $r_0^s = R_\odot/10.37$ where $R_\odot = 6.96 \times 10^{11}$ m is the average radius of the Sun; see Fig. 8 for a comparison of the matter potential in the standard case (left) and in the scenario of interest here (right, labeled sterile neutrino).

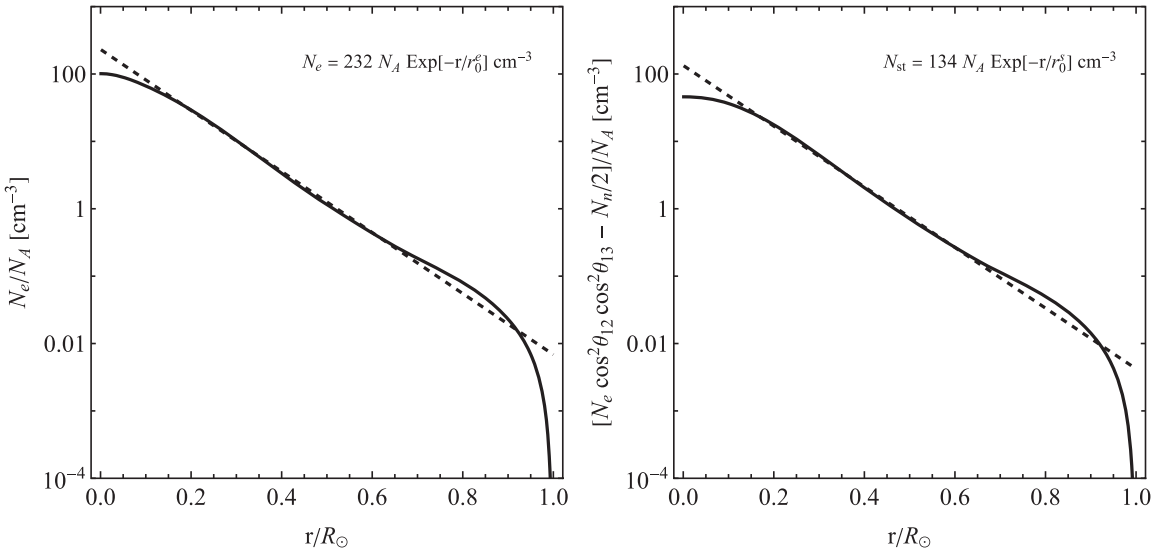

FIG. 8. Solar matter potential for active (left) and sterile (right) neutrinos—the scenario of interest here—as function of the distance from the center in units of the Solar radius, from the B16-GS98 Solar Model [4]. We also present our fitted exponential forms, where $r_0^e = R_\odot/10.43$, and $r_0^s = R_\odot/10.37$, in dashed lines.

[1] J. Aalbers *et al.* (DARWIN Collaboration), Solar neutrino detection sensitivity in DARWIN via electron scattering, Eur. Phys. J. C **80**, 1133 (2020).

[2] J. N. Bahcall, M. H. Pinsonneault, and S. Basu, Solar models: Current epoch and time dependences, neutrinos, and helioseismological properties, Astrophys. J. **555**, 990 (2001).

[3] A. M. Serenelli, W. C. Haxton, and C. Pena-Garay, Solar models with accretion. I. Application to the solar abundance problem, Astrophys. J. **743**, 24 (2011).

[4] N. Vinyoles, A. M. Serenelli, F. L. Villante, S. Basu, J. Bergström, M. C. Gonzalez-Garcia, M. Maltoni, C. Peña Garay, and N. Song, A new generation of standard solar models, Astrophys. J. **835**, 202 (2017).

[5] G. Bellini *et al.* (BOREXINO Collaboration), Neutrinos from the primary proton–proton fusion process in the Sun, Nature (London) **512**, 383 (2014).

[6] L. Wolfenstein, Different varieties of massive Dirac neutrinos, Nucl. Phys. **B186**, 147 (1981).

[7] S. T. Petcov, On pseudodirac neutrinos, neutrino oscillations and neutrinoless double beta decay, Phys. Lett. **110B**, 245 (1982).

[8] S. M. Bilenky and B. Pontecorvo, Neutrino oscillations with large oscillation length in spite of large (Majorana) neutrino masses?, Sov. J. Nucl. Phys. **38**, 248 (1983), https://lib-extopc.kek.jp/preprints/PDF/1983/8305/8305369.pdf.

[9] A. de Gouvêa, W.-C. Huang, and J. Jenkins, Pseudo-Dirac neutrinos in the new standard model, Phys. Rev. D **80**, 073007 (2009).

[10] A. Donini, P. Hernandez, J. Lopez-Pavon, and M. Maltoni, Minimal models with light sterile neutrinos, J. High Energy Phys. 07 (2011) 105.

[11] A. de Gouvêa, I. Martinez-Soler, Y. F. Perez-Gonzalez, and M. Sen, Fundamental physics with the diffuse supernova background neutrinos, Phys. Rev. D **102**, 123012 (2020).

[12] I. Martinez-Soler, Y. F. Perez-Gonzalez, and M. Sen, SN1987A still shining: A quest for pseudo-Dirac neutrinos, Phys. Rev. D **105**, 095019 (2022).

[13] J. Aalbers *et al.* (DARWIN Collaboration), DARWIN: Towards the ultimate dark matter detector, J. Cosmol. Astropart. Phys. 11 (2016) 017.

[14] P. A. Zyla *et al.* (Particle Data Group), Review of particle physics, Prog. Theor. Exp. Phys. **2020**, 083C01 (2020).

[15] I. Esteban, M. C. Gonzalez-Garcia, M. Maltoni, T. Schwetz, and A. Zhou, The fate of hints: Updated global analysis of three-flavor neutrino oscillations, J. High Energy Phys. 09 (2020) 178.

[16] B. Aharmim *et al.* (SNO Collaboration), Combined analysis of all three phases of solar neutrino data from the Sudbury Neutrino Observatory, Phys. Rev. C **88**, 025501 (2013).

[17] K. Abe *et al.* (Super-Kamiokande Collaboration), Solar neutrino measurements in Super-Kamiokande-IV, Phys. Rev. D **94**, 052010 (2016).

[18] H. Nunokawa, S. J. Parke, and R. Zukanovich Funchal, What fraction of boron-8 solar neutrinos arrive at the earth as a nu(2) mass eigenstate?, Phys. Rev. D **74**, 013006 (2006).

[19] G. Bak *et al.* (RENO Collaboration), Measurement of Reactor Antineutrino Oscillation Amplitude and Frequency at RENO, Phys. Rev. Lett. **121**, 201801 (2018).

[20] D. Adey *et al.* (Daya Bay Collaboration), Measurement of the Electron Antineutrino Oscillation with 1958 Days of Operation at Daya Bay, Phys. Rev. Lett. **121**, 241805 (2018).

[21] H. de Kerret *et al.* (Double Chooz Collaboration), Double Chooz θ_{13} measurement via total neutron capture detection, Nat. Phys. **16**, 558 (2020).

[22] P. Adamson *et al.* (NOvA Collaboration), First Measurement of Electron Neutrino Appearance in NOvA, Phys. Rev. Lett. **116**, 151806 (2016).

[23] K. Abe *et al.* (T2K Collaboration), Measurement of neutrino and antineutrino oscillations by the T2K experiment including a new additional sample of ν_e interactions at the far detector, Phys. Rev. D **96**, 092006 (2017); Erratum, Phys. Rev. D **98**, 019902 (2018).

[24] A. de Gouvêa and K. J. Kelly, Neutrino vs antineutrino oscillation parameters at DUNE and Hyper-Kamiokande, Phys. Rev. D **96**, 095018 (2017).

[25] A. de Gouvêa, A. Friedland, and H. Murayama, The dark side of the solar neutrino parameter space, Phys. Lett. B **490**, 125 (2000).

[26] C. Giunti and K. C. Wook, *Fundamentals of Neutrino Physics and Astrophysics* (Oxford University, Oxford, 2007).

[27] F. An *et al.* (JUNO Collaboration), Neutrino physics with JUNO, J. Phys. G **43**, 030401 (2016).

[28] K. Goldhagen, M. Maltoni, S. Reichard, and T. Schwetz, Testing sterile neutrino mixing with present and future solar neutrino data, Eur. Phys. J. C **82**, 116 (2022).

[29] S. T. Petcov, Exact analytic description of two neutrino oscillations in matter with exponentially varying density, Phys. Lett. B **200**, 373 (1988).

[30] A. de Gouvêa, in *Theoretical Advanced Study Institute in Elementary Particle Physics: Physics in* $D \geqq 4$ (TASI, Boulder, USA, 2004).

[31] A. Friedland, On the evolution of the neutrino state inside the sun, Phys. Rev. D **64**, 013008 (2001).

[32] P. C. de Holanda and A. Y. Smirnov, Homestake result, sterile neutrinos and low-energy solar neutrino experiments, Phys. Rev. D **69**, 113002 (2004).

[33] P. C. de Holanda and A. Y. Smirnov, Solar neutrino spectrum, sterile neutrinos and additional radiation in the Universe, Phys. Rev. D **83**, 113011 (2011).

[34] H. Murayama, Impact of neutrino oscillation measurements on theory, AIP Conf. Proc. **721**, 122 (2004).